High Energy Processes in Accreting Black Holes
ASP Conference Series, Vol. 161, 1999
Juri Poutanen and Roland Svensson, eds.

Accretion Disks in the Context of Self-Organized Criticality: How to Produce $1/f$ Fluctuations?

Shin Mineshige

Department of Astronomy, Graduate School of Science, Kyoto University, Sakyo-ku, Kyoto 606-8502, Japan; E-mail: minesige@kusastro.kyoto-u.ac.jp

Hitoshi Negoro

Institute for Physical and Chemical Sciences (RIKEN), 2–1 Hirosawa, Wako, Saitama 315-0198, Japan; E-mail: negoro@crab.riken.go.jp

Abstract. Rapid fluctuations with a frequency dependence of $f^{-\beta}$ with $\beta \sim 1$ are commonly observed in the radiation from stellar black-hole candidates and active galactic nuclei. To understand the origin of such $1/f$-like fluctuations, we introduce the notion of the *self-organized criticality* (SOC), one of the central dogmas for understanding the behavior of complex systems exhibiting $1/f$ noise. We assume that a disk becomes locally unstable where mass density exceeds some critical value and that the result of the instability is an avalanche accretion flow towards the center. Then, the disk spontaneously evolves to and steadily stays at an SOC state, in which, any size of avalanches can be produced. With this model we can reproduce $1/f$-like fluctuations as are observed, not critically depending on a detailed mechanism for creating disturbances.

1. Introduction

One of the most well-known features commonly observed in both Galactic black-hole candidates (BHCs) and Seyfert 1 type AGNs is rapid variability (see reviews by Oda 1977, van der Klis 1995 for Galactic BHCs; Wallinder et al. 1992, Ulrich et al. 1997 for AGNs and references therein).

To obtain a rough idea of how variability light curves look, we display a typical example of fluctuating light curves for the case of Cyg X-1 in Figure 1. Note the apparently self-similar fluctuation patterns on different timescales. The light curves are neither periodic nor random around some mean. Rather, the light curves look like an ensemble of numerous shots (or peaks) with a variety of durations and peak intensities. Similar light curves are obtained for AGNs. Below we summarize the generic properties of the fluctuations.

1. In BHCs, the fluctuation properties are closely related to the spectral state of the accretion disks. Rapid X-ray fluctuations are more pronounced during the hard (low) state although there exist small fluctuations during

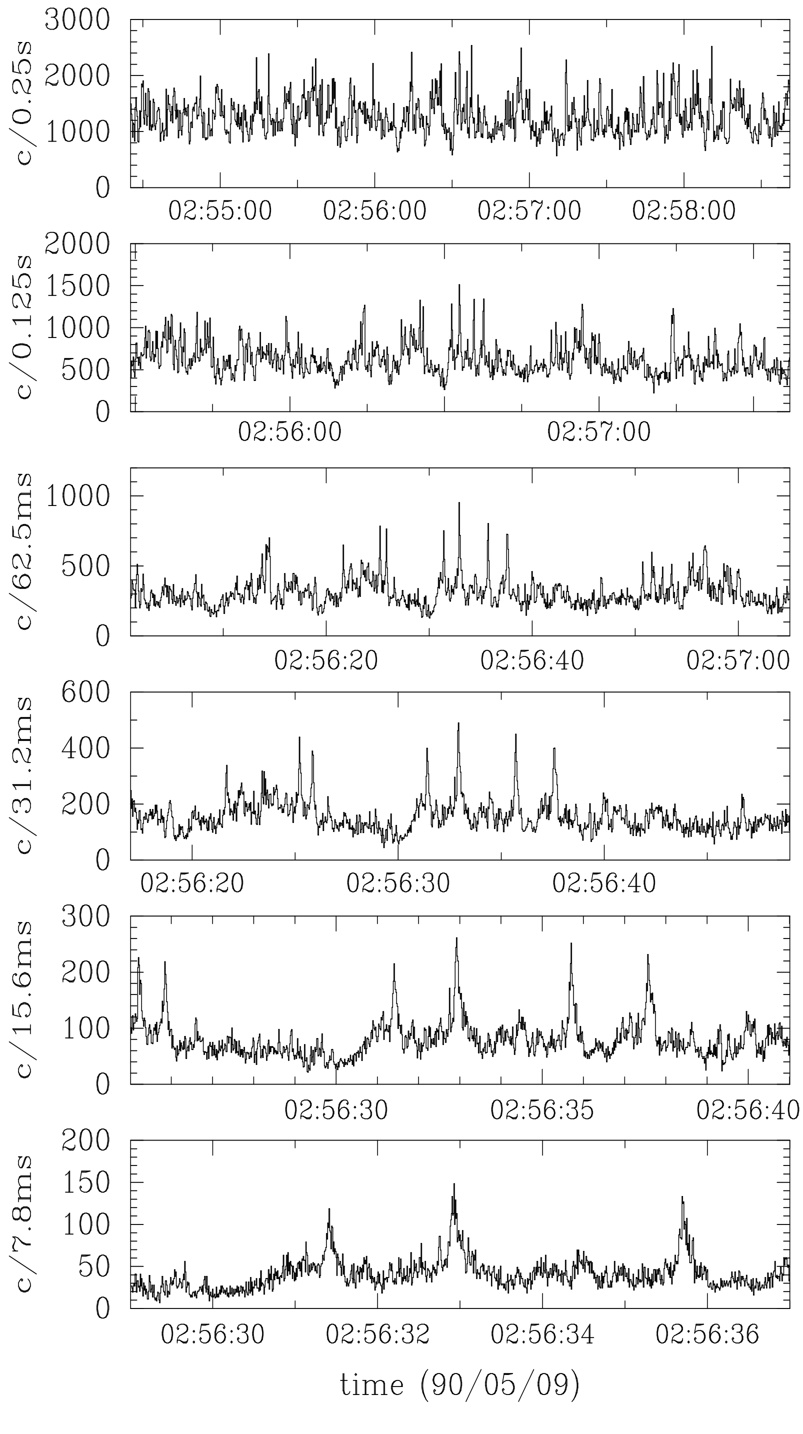

Figure 1. X-ray light curves of Cyg X-1 observed with *Ginga* during its hard state (from Negoro 1995).

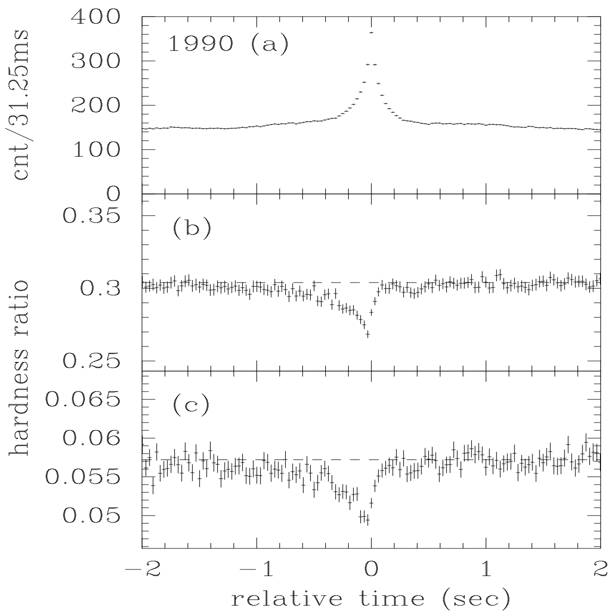

Figure 2. Superposed shot profile (upper) and hardness ratios (lower) calculated from the light curves of Cyg X-1 (from Negoro 1995). Corresponding energy ranges are (a) 1.2–36.8 keV (b) 6.9–13.8 keV/1.2–6.9 keV, (c) 13.8–23.0 keV/1.2–6.9 keV, respectively.

the soft state, as well (Miyamoto et al. 1992, 1993). In AGNs, variability amplitude seems to depend on the luminosity.

2. Through an analysis using an *auto-correlation function* (ACF) of light curves of Cygnus X-1, it was suggested that the observed variations are consistent with a random shot-noise model (Terrell 1972). However, there is a smooth number distribution of shots against peak intensity (Negoro et al. 1995) and duration (Focke 1998).

3. Negoro et al. (1994) superposed the shot time profiles by aligning the peaks of large shots. Figure 2 displays the superposed shot profile (upper panel) and its hardness ratios (middle and lower panels). Clearly, a shot profile is sharply peaked and rather (time) symmetric. Note also gradual spectral softening in the rise and sudden hardening around the peak.

4. The *power spectral density* (PSD) consists of a flat part at low frequencies and a power-law decline part at high frequencies, $\propto f^{-\beta}$, where f is the frequency and $1 < \beta \lesssim 2$ (see Lochner et al. 1991; Miyamoto et al. 1993; Lawrence & Papadakis 1993, Hayashida 1999). Figure 3 illustrates the PSD of Cygnus X-1 light curves. As is shown here, the gradual decline part ($0.1 \lesssim f \lesssim 1.0$) of the observational PSDs is determined by the mean time profile of the large shots (Negoro et al. 1994).

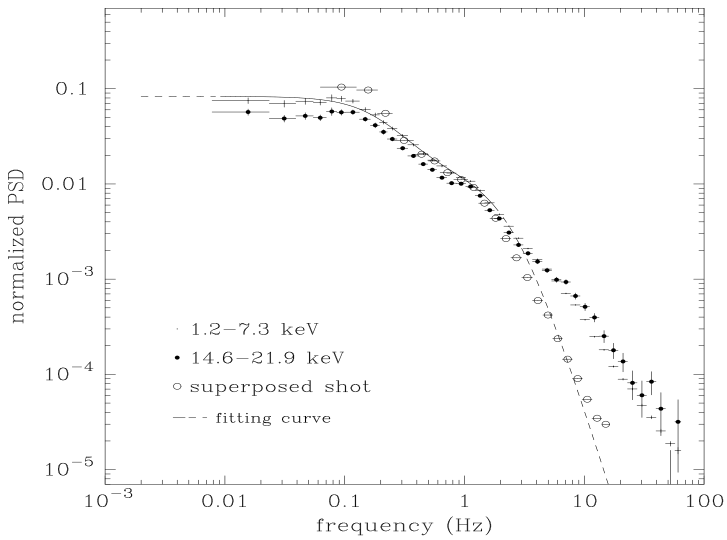

Figure 3. PSDs calculated from the light curves of Cyg X-1 (Negoro 1995). Open circles are a PSD of a superposed shot (see fig. 2).

5. For Cyg X-1, hard photons generally lag the soft ones by several to tens of milliseconds, and the time delay increases almost linearly with the Fourier period (Miyamoto et al. 1988, 1993).

Long before detailed PSD analyses were performed, Press (1978) already noted that the (optical) quasar light curve appears to be somehow 'in between' the white noise (f^0 noise) and the random-walk noise ($1/f^2$ noise; a running sum of the white-noise process). Flicker ($1/f$) noise is a good example. By definition, white noise has no time correlation. Random-walk noise has a strong short-term correlation in the sense that the value at a certain time totally depends on the value at the previous time step. Flicker noise, in contrast, has a weak, short-term correlation.

Then, how can flicker noise arise under realistic circumstances? As Press (1978) pointed out, one can generate $1/f$-like fluctuations by superimposing the shot light curves with different peak intensities and lifetimes, if they have a power-law dependence on the radius (Meekins et al. 1984, Lehto 1989). Of course, we can construct a model by simply assuming the power-law relations. However, such a model is not fully convincing. We wish to know how nature works; why does nature prefer power-law distribution of peak intensities, lifetimes, and so on? Let us, next, turn our eyes onto the recent progress made in the field of the complex systems.

2. Cellular Automaton Model for Fluctuations

We conjecture here that light fluctuations originate from different parts of the disk; if so, a weak time correlation in the light curves indicates weak spatial communication (or coherency) among different sites in the disk. The technique of cellular automata is useful to model such a weak spatial coherency.

2.1. Smooth Number Distribution of Shot Sizes

What is the significance of the smooth number distribution of shots against the peak-intensity (item 2. above)? This is difficult to understand in the framework of usual physics, since according to the usual way of thinking in physics we should first estimate physical quantities, such as density and temperature, evaluate time and length scales, and discuss relevant physical mechanisms. In other words, the system in question should have typical scales.

In nature, in contrast, smooth size distribution is often observed. Consider earthquakes, for example; the number of earthquakes is known to exhibit a power-law distribution against their magnitudes, from frequent small earthquakes to rare big ones. Solar flares are another good example (Dennis 1985). In fact, there are *no typical scales* there.

Then, how can such a scale invariance arise naturally? Recent studies of nonlinear physics tell that an important key is *non-equilibrium*. A good example is a limit cycle (see Fig. 4) or a reservoir, in which even if a mass-input is constant, mass output will be episodic. However, this is not enough; another important key is *interactions* (or *couplings*). Suppose that we connect numerous limit-cycle oscillators in such a way that an output of one limit cycle becomes an input of others in the down-stream (see the right panel of Fig. 4). What then happens?

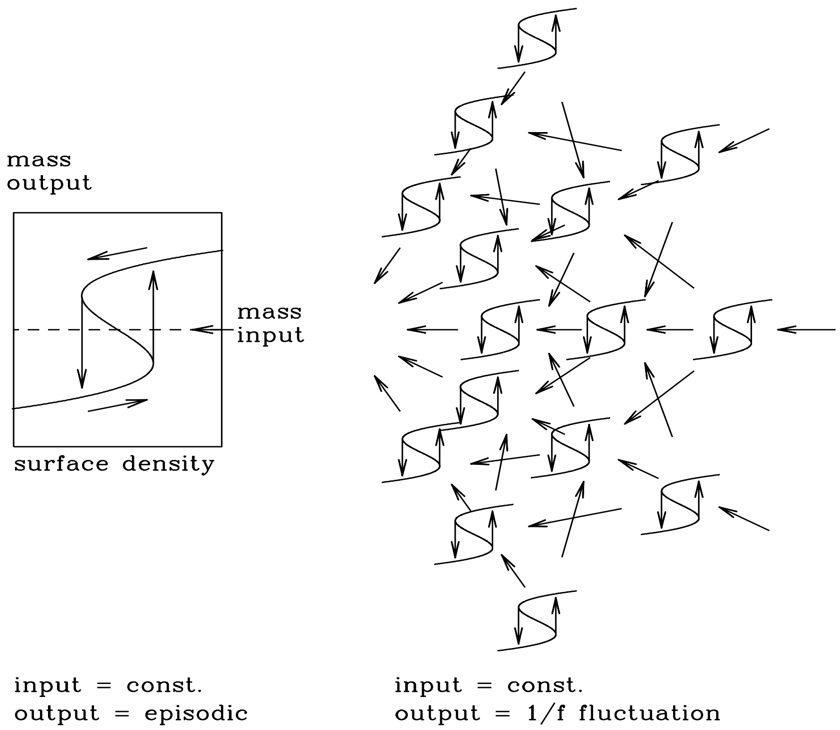

Figure 4. When a disk undergoes limit cycles (see left panel), the mass output will be episodic, even when the mass input is constant. If we connect plenty of such limit-cycle oscillators (see right panel), $1/f$ fluctuations can be expected in the total outputs.

2.2. Self-Organized Criticality

A model like a coupled limit-cycle oscillators was first discussed by Bak et al. (1987, 1988). The most outstanding feature of their model is that the system, following a cellular automaton rule, spontaneously evolves to and steadily stays at a critical state. In this state the system produces $1/f$ fluctuations on the energy dissipation, although the energy is injected randomly in time and space. Since this state is spontaneously reached from arbitrary initial conditions, it is called a *self-organized critical state* (SOC state), while the above cellular automaton model is called a sand-pile model, since it roughly describes the dynamics seen on a time-evolving sand mountain. If we add sand grains one by one onto a sand mountain it would eventually cause a large avalanche in some case, but also may cause no avalanche in another case. The size of the avalanche depends on the positions and times that grains are added.

"As the pile is built up, the characteristic size of the largest avalanches grows until at the critical point there are avalanches of all sizes up to the size of the system. The energy is then dissipated at all length scales. Once the critical point is reached, the system stays there" (Bak et al. 1988).

One of the most conspicuous natures of the SOC is its ubiquity; namely, it is supposed to describe the temporal sequence of a wide range of non-equilibrium open systems, such as earthquakes, forest fires, co-evolution of biological species, and traffic flows (Bak 1996). Although the above model is no more than a simple cellular-automaton model, it may lay claim to be a prototype model for various SOC phenomena, and can afford to describe other individual phenomena if properly modified according to the detailed dynamics of the relevant system in question.

2.3. Procedures of a Cellular-Automaton Model

We now modify the sand-pile model by Bak et al. so as to reproduce the observed variability of black-hole objects (Mineshige et al. 1994a, 1994b).

It is usually thought that the disk fluid is continuous and that physical quantities only smoothly vary in space and time. Here, instead, we adopt a coarse-grained description for the inner fluctuating parts (probably advection-dominated parts) of the disk and model their behavior by regarding them as comprising numerous reservoirs with finite capacities. Importantly, if the system is out of equilibrium, such a coarse-grained description does not always tend to a continuous description (in which the system is assumed to be in equilibrium on infinitesimal length scales), even when the number of segments goes to infinity.

The physical assumptions and numerical procedures are as follows:

1. Divide the disk plane into numerous cells along the radial and azimuthal coordinates. For example, the azimuthal coordinates are equally divided into N_φ segments, $\varphi_i, \cdots, \varphi_{N\varphi}$ (say, $N_\varphi = 64$; $\Delta\varphi = 2\pi/64$), while the radial coordinates are also divided into N_r segments, $r_1 \equiv r_{\rm out}, \cdots, r_{Nr} \equiv r_{\rm in}$ (say, $N_r = 64$). Here, $r_{\rm out}$ and $r_{\rm in}$ are the outer and inner edges of (the advection-dominated portions of) the disk.

2. Choose one cell randomly at the outermost ring and put a gas particle with a mass m into that selected site. This process represents mass supply to the disk in question.

3. Define $M_{i,j}$ to be the mass of a cell at (r_i, φ_j). Search for an unstable site in which $M_{i,j} > M_{\rm crit}(r)$, where $M_{\rm crit}$ is an *a priori* given critical mass. [It can be shown that the dynamics is insensitive to the exact functional form of $M_{\rm crit}(r)$.] If found, let three mass particles fall from that cell equally into adjacent three cells at r_{i+1} (see Fig. 5); i.e.,

$$\begin{aligned} M_{i,j} &\rightarrow M_{i,j} - 3m, \\ M_{i+1,j\pm1} &\rightarrow M_{i+1,j\pm1} + m, \\ M_{i+1,j} &\rightarrow M_{i+1,j} + m. \end{aligned} \tag{1}$$

   This process corresponds to an avalanche flow or flare. In some cases, the inner cells may become unstable as the result of an avalanche flow from above. In such a case, a subsequent avalanche flow occurs in the next time step [after completing one cycle of procedures 2. to 5.].

4. Choose randomly one cell at each ring, and let a small amount of mass, $m' \ll m$, fall into the adjacent inner cell with the same φ; that is,

$$M_{i,j} \rightarrow M_{i,j} - m', \quad M_{i+1,j} \rightarrow M_{i+1,j} + m'. \tag{2}$$

   This procedure, corresponding to gradual (one-sided) viscous diffusion, should be accomplished regardless of whether $M_{i,j} > M_{\rm crit}$ or not. This was not included in the original model by Bak et al., however, without diffusion one cannot produce $1/f$ fluctuations but just $1/f^2$ fluctuations.

5. Calculate the gravitational energy dissipated by mass accretion, assuming that a certain fraction of the dissipated energy is converted to radiation. Note that if the disk is advection-dominated, radiation loss is not always proportional to the dissipated energy, though the results do not sensitively depend on this.

6. Repeat processes 2. to 5. for over 10^5 times. This is to remove any initial transient states and to minimize any statistical errors.

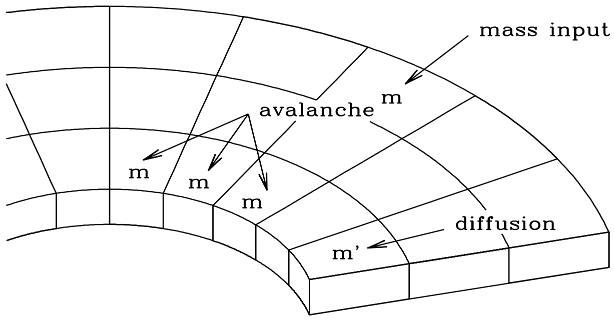

Figure 5. Cellular automaton rule for the SOC model for variability. The rule consists of (1) mass accretion flow into a disk, (2) an avalanche and (3) gradual (one-sided) diffusion.

We may start calculations either from an empty disk or from the marginally stable state (in which $M_{i,j} = M_{\rm crit}$), since the results do not depend on the initial state (see subsection 2.5). As we add particles into the outermost ring, matter piles up there and occasionally slides into inner regions when the mass density exceeds the critical value.

2.4. Properties of the SOC State

The system which evolved to the SOC-state shows some characteristic features, as described below (cf. Bak et al. 1988; Takeuchi et al. 1995).

1. The light curves consist of numerous events with sharp peaks or shots.
2. The PSD obeys a power-law in the high-frequency region.
3. The peak intensity of shots, the total dissipated energy per shot, and the lifetime of shots are smoothly distributed.
4. Non-random (temporal) distribution of large shots. The occurrence of large shots is suppressed for a certain period after one large shot.

Let us discuss below these features in more details.

Light curve and PSD Figure 6 illustrates typical examples of the light curves (left panels) and the PSD (right panel) simulated based on the SOC model. Shots with different peak intensities and time durations seem to appear randomly in time. The PSD consists of a flat-top part at low frequencies and a power-law decline part with $1/f^\beta$ at high frequencies, as in the observational PSDs. As m' increases, the occurrence of large events (shots) tends to be suppressed, and accordingly, the decline part of the PSD becomes flatter; the power-law index changes as $\beta \sim 1.9, 1.7, 1.5$, and 1.1, for $m' = 0$, $m/100, m/10$, and $m/5$, respectively. The model with $m' = m/10$ gives the best fit to the observed PSD shape and the configuration of the light curve (see Fig. 6). Note that the inclusion of relativistic corrections, such as relativistic boosting, tends to reduce β when the inclination angle is small (Abramowicz and Bao 1994).

Shot (peak) intensity distribution We calculated the number of shots, $D(p)dp$, using peak intensities between p and $p + dp$ from simulations data based on the SOC model. A plot of the results is given in the left-hand panel of Figure 7. The vertical axis represents the relative values. Quite generally, the peak intensity of an individual shot shows a smooth, power-law distribution. We plot here the case with $m' = m/10$, since it gives the best fit to the observations (see below).

As we have seen concerning the PSDs, the magnitude of a gradual mass flow (m'/m) also affects the shape of the peak-intensity distribution. As it becomes enhanced, $D(p)$ becomes steeper in the large-p region, and $D(p)$ becomes more like an exponential than like a power law. (Strict speaking, this is no longer a critical state, since a critical state, by definition, means a power-law distribution.) If we fit $D(p)$ at large peak intensities by a power-law, $D(p) \sim p^{-s}$, the power-law indices are, $s \sim$ 5.6, 7.7, and 11.5 for $m' = m/100, m/10$, and $m/5$, respectively.

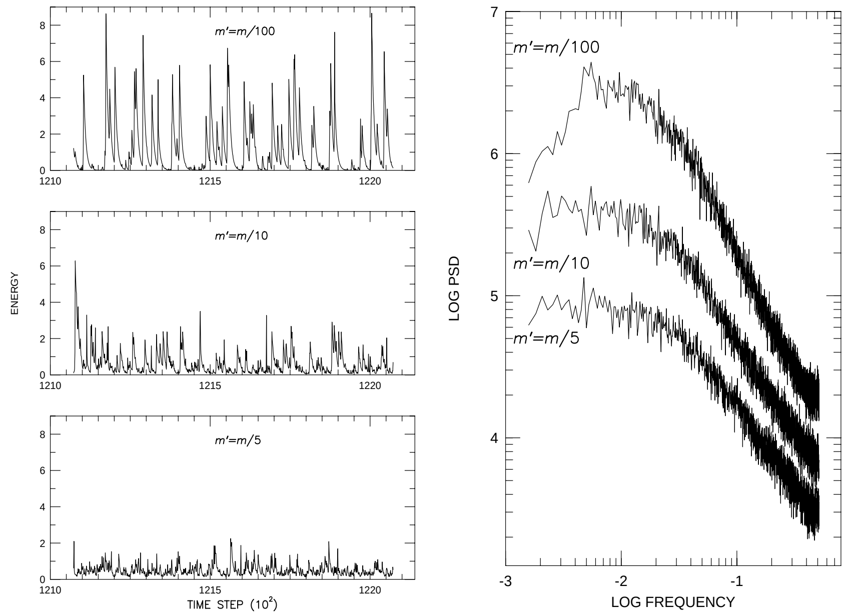

Figure 6. Typical light curves (left) and the power-spectral density (right) calculated based on the SOC models with $m'/m = 1/100$, $1/10$, and $1/5$, from top to bottom, respectively (from Takeuchi et al. 1995).

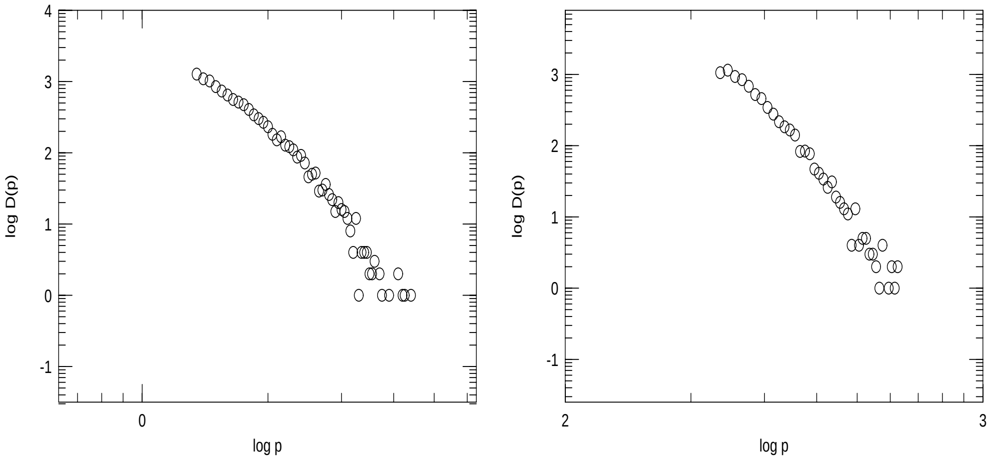

Figure 7. Theoretical (left) and observational (right) peak-intensity distribution of shots. The shots with a peak intensity greater than 1.5-times the local mean intensity are selected in the observations (Negoro et al. 1995).

For a comparison we also calculated the peak-intensity distribution for the *Ginga* data of Cyg X-1 (Fig. 1); the results are plotted in the right-hand panel of Figure 7. The observation shows an exponential distribution suggesting that m'/m is large. If the distribution is represented with a power law, its index is $s \sim 7.1$ for $p \geq 350$ count/s, which is again in good agreement with the model with $m' \sim m/10$.

The disk remaining in the SOC state yields a variety of avalanche flow, both in the peak intensities and in the durations, for the following reason (see Fig. 8). In most cases, one single flare does not induce another flare, since the adjacent sites are not marginally unstable (the masses there are well below their critical values). However, a flare may occasionally trigger avalanche flow over several radial mesh points, if some of the adjacent cells are marginally unstable (the mass densities there are barely below the critical values). The probability of one avalanche to initiate another one thus depends on how close the mass densities in the inner rings are to their critical values. The process is quite stochastic. As a result, there are many small shots. Among them, somewhat larger shots occasionally appear. For a long run, an even larger shot occurs. The system is not regular nor purely chaotic; such a state is sometimes called as *edge of the chaos.*

Shot (peak) interval distribution We finally address the following question: do the shots occur at random or not? This is essential to discriminate a simple shot model (cf. Terrell 1972) from ours, since the former predicts a random appearance of shots, while the latter requires that the occurrence of a large flare is suppressed just after the previous large flare (Negoro et al. 1995).

We have found (Takeuchi et al. 1995) that in both the theory and observations the occurrence of large shots is suppressed within a certain interval (which we call the waiting time) after the previous large shot. Interestingly, the waiting time is an increasing function of the peak intensity (or the total energy release) of the shots. From the observations of Cygnus X-1, we find the waiting time to be $\sim$ 10 s for relatively large shots and $\sim$ 5–6 s for smaller shots. Small shots, in contrast, tend to occur nearly at random.

The reason for non-random distribution of shots is as follows. Since the amount of mass dissipated by a single, small event is small, a small shot does not affect the entire mass distribution over the disk plane. Therefore, the site which becomes unstable in the next time step depends totally on where to put the next mass particle. The procedure to put the next mass particle is a stochastic process. Thus, small shots occur at random. When a large event occurs, a large hole is created afterwards, since a large amount of gas is dissipated (see the lower-right panel of Fig. 8). A longer time is thus needed to refill a hole with gas until the next large event can take place. Large shots thus occur non-randomly.

Although it appears as if X-ray shots of Cyg X-1 occur at random, we now confirm that this is not the case.

2.5. Remarks Concerning the SOC Model

There seem to be many model parameters in our model, but we stress here that results are rather insensitive to most of them. We may modify the avalanche rule; for example, the number of the mass particles falling into the inner cells

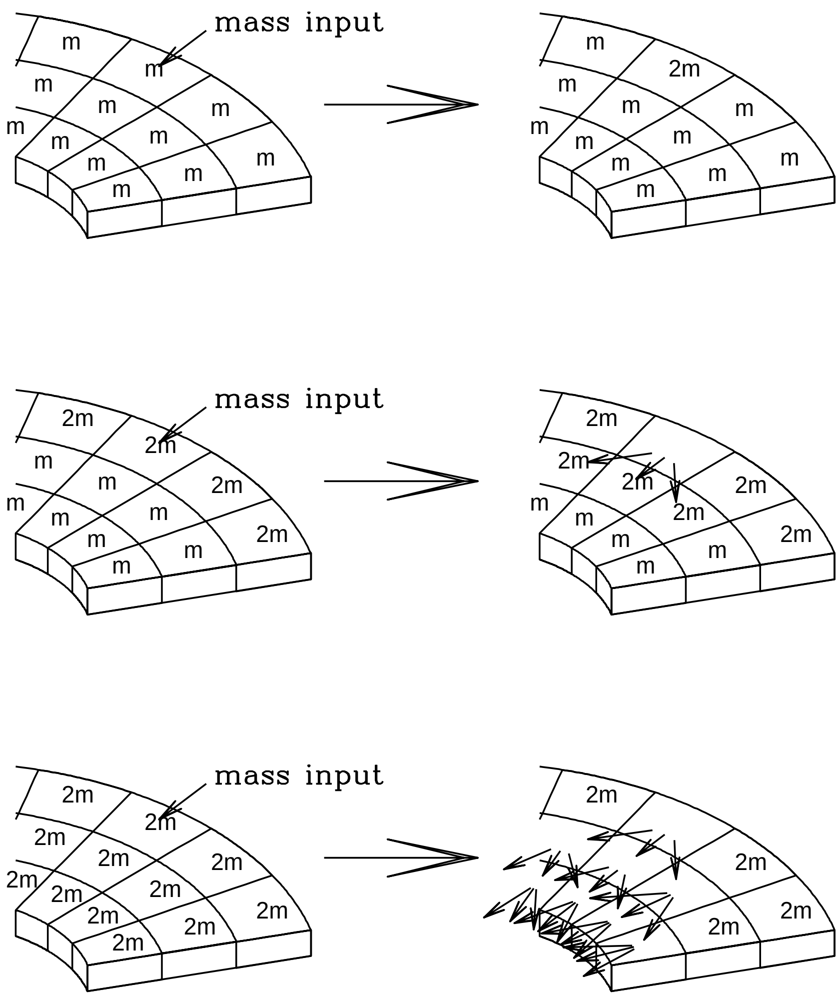

Figure 8. A variety of an avalanche flow in a disk in the SOC state. Here, we assume $M_{\rm crit} = 2m$. If mass density is everywhere m, there will be no avalanche in the next step (see upper two panels). If mass density is $2m$ in the outermost ring and is m otherwise, one-step avalanche will be triggered in the next step (see middle panels). If mass density is everywhere $2m$, an addition of an infinitesimal mass causes a large-scale avalanche over the entire disk plane (see lower panels). The number of cells involved with an avalanche increases from the top to the bottom, while the probability of producing avalanches decreases downward.

can be changed. We may rotate the inner parts in accordance with differential rotations (mimicking the shear in the disk). Likewise, you may change the prescription of the critical mass as you like, and can also change the size and number of cells. It can be demonstrated that the power-law slopes of PSD are rather insensitive to the strict rule for an avalanche (see Takeuchi et al. 1995).

There are two important parameters: m'/m (ratio of the diffusion rate to the avalanche flow rate) and the size of (the fluctuating part of) the disk. The former sensitively changes the power-law slope in the PSD, while the latter determines the break frequency in the PSD (shown later).

We cannot, however, assume a one-dimensional (1D) avalanche flow instead of the two-dimensional (2D) or three-dimensional (3D) flows, as assumed here. In fact, a 1D avalanche should always trigger another avalanche in the adjacent inner ring (so-called "domino effects"), because the inner ring catches 100% of the enhanced mass flow by the avalanche from above (except at initial transient states). The consequences are sporadic outbursts of similar (very large) amplitude.

2.6. Generation of $1/f$ Fluctuation Spectra

The reason for producing a $1/f$-like fluctuation by our model can be naively explained as follows. Quite generally, the PSD of a single shot light curve has a f^{-2} decline or an even steeper one. If a shot has an exponential decay, $p\exp(-t/\tau)$ for $t \geq 0$ with τ being a time constant, for example, its PSD is the so-called Lorentzian profile which has a f^{-2} decline at $f > 1/(2\pi\tau)$;

$$S_\tau(f) = p^2 \frac{\tau^2}{1 + 4\pi^2\tau^2 f^2}. \tag{3}$$

If the time profile is time-symmetric exponentials, $p\exp(-|t|/\tau)$, the PSD of each shot has a $1/f^4$ decline at high frequencies. This means, it is difficult to reproduce $1/f$-like declines by a single shot profile. We need to superpose many different shot profiles.

Figure 9 schematically explains how $1/f$-like PSD are reproduced by the superposition of individual shots with various peak intensities and lifetimes. In such $1/f$-like PSDs, large and longer shots contribute to the low-frequency PSD, while small and shorter shots determine the power-law decline at high frequencies. Now we understand that the $1/f$-like decline in the PSD is a result of the superposition. In other words, variations in shot durations are essential. Importantly, the $1/f$-like slope is not sensitive to the slope in the PSD of individual shots, since the contribution of a shot with a duration τ to the entire PSD is practically negligible at $f > 1/(2\pi\tau)$.

Then, what does the break frequency, $f_{\rm break}$, stand for? In our model it is the inverse of the duration of the biggest events; i.e., the accretion time from the outer boundary (of the fluctuating part) of the disk. If we denote this radius as $r_{\rm out}$, and if the accretion timescale ($\tau_{\rm acc}$) is by a factor of 3–10 longer than the free-fall timescale, $\tau_{\rm ff}$ (as is the case for advection-dominated flows), we find

$$r_{\rm out} = (GM\tau_{\rm ff}^2)^{1/3} \simeq 10^{8.5} \left(\frac{\tau_{\rm acc}}{10\tau_{\rm ff}}\right)^{-2/3} \left(\frac{f_{\rm break}}{0.1{\rm Hz}}\right)^{-2/3} \left(\frac{M}{10M_\odot}\right)^{1/3} {\rm cm}. \tag{4}$$

That is, the boundary is at $r_{\rm out} \sim 100 r_{\rm S}$ ($r_{\rm S}$ is the Schwarzschild radius).

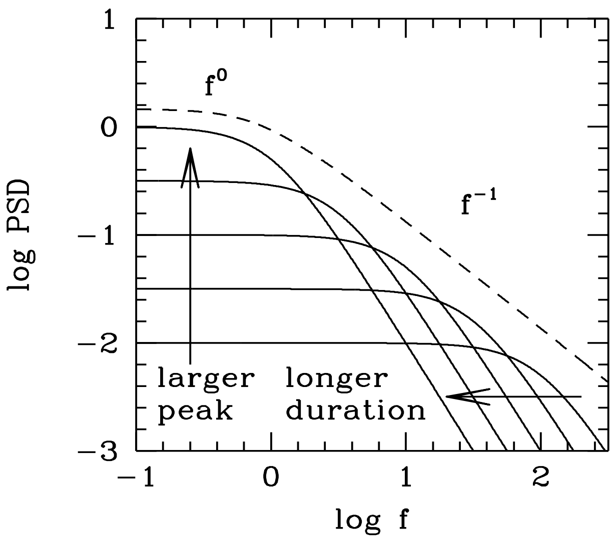

Figure 9. Schematic view of $1/f$-like power spectral density (PSD). The superposition of the individual shots with various energy and lifetime produces a $1/f$-like PSD (from Takeuchi et al. 1995).

3. Discussion

3.1. Origin of Criticality?

So far, we did not specify an underlying mechanism of the instability. What is it likely to be? It seems that instabilities are somehow related to magnetic fields. There are number of reasons for this. Any magnetic systems, including solar coronae (Ueno et al. 1997), fusion tokamak (Carreras et al. 1996), and recently performed 3-dimensional MHD simulations (Matsumoto et al. 1998), all show $\sim 1/f$ fluctuations in their outputs. Then, what is a mechanism? The most promising possibility at present is magnetic reconnection leading to magnetic flares, similar to solar flares (Wheeler 1977; Galeev et al. 1979; Takahara 1979). It is very instructive to note the power-law dependence of the flare occurrence rate on the flare size (Dennis 1985). This may indicate the solar coronal magnetic fields being in a self-organized state in a sense similar to a sand pile (Lu and Hamilton 1991). As energy goes into a system, magnetic field strength and, hence, electric current and drift velocity increase, a situation easy to turn on anomalous resistivity, thereby starting magnetic reconnection.

The similar mechanism is also feasible in a disk, because the existence of stronger differential rotation favors to strengthen the magnetic fields in the disk. The presence of magneto-hydrodynamical (MHD) instabilities also stimulates amplification of the fields. The advection-dominated disk is favored for our model, since it is characterized by low emissivity (due to usual thermal emission) and a large infall velocity (sometimes comparable to the azimuthal velocity). The main energy release thus occurs by sporadic reconnection events (Mineshige et al. 1995).

3.2. Importance of Cellular-Automaton Simulations

In this article, we constructed a simple cellular-automaton model and tried to reproduce the observed properties of the variability. Good agreements were obtained for some statistical properties, such as the shape of the power spectra and peak-intensity distributions. Obviously, we cannot deal with any hydrodynamical effects with a cellular-automaton model. Then, why do we stick to such a rather idealized model?

We believe that our SOC model is useful in two ways. One is that we can use the cellular-automaton simulations as a $1/f$-like noise generator. With the SOC model we can simulate how blobs, responsible for fluctuations, form and are destroyed. We can produce avalanche flows with arbitrary lifetimes and peak intensities, not critically depending on detailed disk structure. We can use such simulations results, when discussing how the properties of intrinsic variations are affected by some other effects, such as gravitational microlensing.

The second advantage is more practical one. Suppose that the real cause of variability is three-dimensional complex behavior of magnetic fields. How can we prove? We may use the notion of the SOC when analyzing the 3D behavior of magnetic fields. For example, the SOC model predicts fractal distribution of any field quantities, such as magnetic field strengths. We can also check if magnetic fields can indeed ignite local instabilities when energy is stored up to a certain limit.

3.3. Time Symmetry and Hard Lag of Shots

Although we present our model for $1/f$-like fluctuation spectra, there remain many unanswered questions; e.g., the time symmetric shot profile and significant hardening occurring around the peak (see Fig. 2). Their origins are not well understood, but we suspect that these might be due to a wave reflection and resultant heating (Manmoto et al. 1996). In an optically-thin, advection-dominated disks a thermal perturbation tends to grow as it moves inward, and eventually it is reflected at the transonic radius as an outgoing acoustic wave. This reflection will produce a time-symmetric profile and cause a hard lag.

Then, as in the case of PSD, the observed hard lag (Miyamoto et al. 1988) may also be well understood in terms of superposed shots (Negoro 1995). In fact, Figure 10 shows that the observed time lags at $f \lesssim 1$Hz are basically reproduced by the time lags of the superposed (average) shots. There are some discrepancies at high frequency sides (with $f > 1$Hz) where small shots seem to contribute. Again, the smooth distribution of shots seem to be important to understand the entire hard-lag diagram.

Acknowledgments. One of the authors (S.M.) would like to thank to Juri Poutanen, Roland Svensson, and Yamada Science Foundation for supports.

References

Abramowicz, M. A., & Bao, G. 1994, PASJ, 46, 523

Bak, P. 1996, How Nature Works, New York: Springer-Verlag

Bak, P., Tang, C., & Wiesenfeld, K. 1987, Phys. Rev., 59, L381

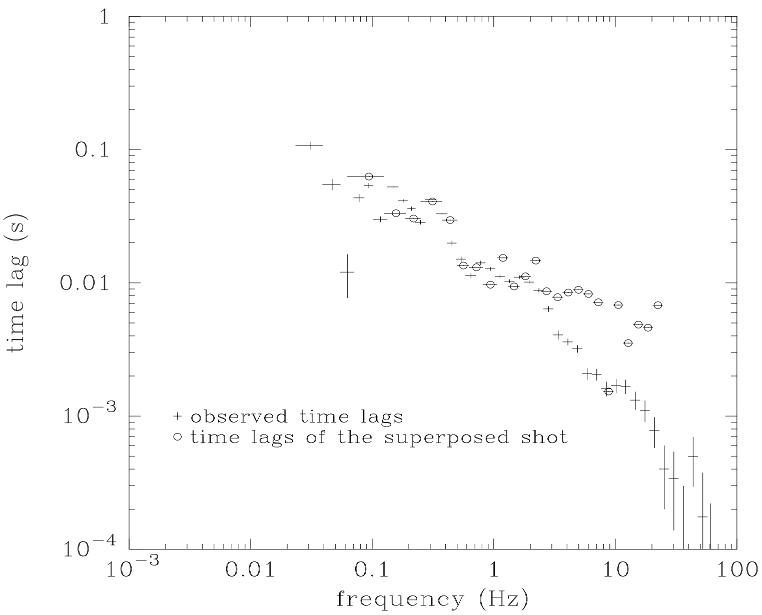

Figure 10. Hard time lags of Cygnus X–1 (from Negoro 1995). Observed time lags and those of the superposed shot are denoted by points with 1σ errors and open circles, respectively. All these indicate hard X-ray lags.

Bak, P., Tang, C., & Wiesenfeld, K. 1988, Phys. Rev. A, 38, 364

Carreras, B. A., Newman, D., Lynch, V. E., & Diamond, P. H. 1996, Phys. Plasmas, 3, 2903

Dennis, B. R. 1985, Solar Phys. 100, 465

Focke, W. B. 1998, Ph.D. Thesis, University of Maryland

Galeev, A. A., Rosner, R., & Vaiana, G. S. 1979, ApJ, 229, 318,

Hayashida, K. 1999, ApJ, in press

Lawrence, A., & Papadakis, I. 1993, ApJ, 414, L85

Lehto, H. J. 1989, In Proc. 23rd ESLAB Symp. on Two Topics in X-ray Astronomy, J. Hunt & B. Battrick, Dordrecht, ESA SP-296, 499

Lochner, J. C., Swank, J. H., & Szymkowiak, A. E. 1991, ApJ, 375, 295

Lu, E. T., & Hamilton, R. J. 1991, ApJ, 380, L89

Manmoto, T., Takeuchi, M., Mineshige, S., Matsumoto R., & Negoro, H. 1996, ApJ, 464, L135

Matsumoto, R. et al. 1999, in preparation

Meekins, J. F. et al. 1984, ApJ, 278, 288

Mineshige, S., Kusunose, M., & Matsumoto, R. 1995, ApJ, 445, L43

Mineshige, S., Ouchi, N.B., & Nishimori, H. 1994a, PASJ, 46, 97

Mineshige, S., Takeuchi, M., & Nishimori, H., 1994b, ApJ, 435, L125

Miyamoto, S., Iga, S., Kitamoto, S., & Kamado, Y. 1993, ApJ, 403, L39

Miyamoto, S., & Kitamoto, S. 1989, Nature, 342, 773

Miyamoto, S., Kitamoto, S., Iga, S., Negoro, H., & Terada, K. 1992, ApJ, 391, L21

Miyamoto, S., Kitamoto, S., Mitsuda, K., & Dotani, T. 1988, Nature, 336, 450

Negoro, H. 1995, Ph.D. Thesis, Osaka University/ISAS Research Note No.616

Negoro, H., Miyamoto, S., & Kitamoto, S. 1994, ApJ, 423, L127

Negoro, H., Kitamoto, S., Takeuchi, M., & Mineshige, S. 1995, ApJ, 452, L49

Oda, M. 1977, Space Sci. Rev. 20, 757

Press, W. H. 1978, Comm. Astrophys. 7, 4

Takahara, F. 1979, PTP, 62, 629

Takeuchi, M., Mineshige, S., & Negoro, H. 1995, PASJ, 47, 617

Terrell, N. J. 1972, ApJ, 174, L35

Ulrich, M.-H., Maraschi, L., & Urry, C. M. 1997, ARA&A, 35, 445

Ueno, S., Mineshige, S., Negoro, H., Shibata, K., & Hudson, H. S. 1997, ApJ, 484, 920

van der Klis, M. 1995, in W. H. G. Lewin, J. van Paradijs & E. P. J. van den Heuvel, Cambridge: Cambridge Univ. Press, 58

Wallinder, F. H., Kato, S., & Abramowicz, M. A. 1992, A&A Rev., 4, 79

Wheeler, J. C. 1977, ApJ, 214, 560